# Effect of Ti-Doping on Thermo-Optical and Electronic Properties of $WS_2$ Nanosheets

**Fatima Matroodi[a,b,*], Ali Ahmadi[a], Morteza Zargar Shoushtari[a], Humberto Cabrera[c,*]**

**[a]Physics Department, College of Science, Shahid Chamran University of Ahvaz, Ahvaz, Iran**
**[b]Center for Research on Laser and Plasma, Shahid Chamran University of Ahvaz, Ahvaz, Iran**
**[c]Optics Lab, The Abdus Salam International Centre for Theoretical Physics (ICTP), Strada Costiera 11,Trieste 34151, Italy**

**Corresponding author email:** f.matroodi@scu.ac.ir, hcabrera@ictp.it

**Regular paper:** Received: Feb. 02, 2022, Revised: Jul. 15, 2022, Accepted: Jul. 24, 2022,
Available Online: Jul. 26, 2022, DOI: 10.52547/ijop.16.1.9

**ABSTRACT— Ti-doped tungsten disulfide ($WS_2$) nanosheet-semiconductor is studied for thermo-optical and electronic properties. Thermal diffusivity (*D*) thermal conductivity (κ) and absorbance were determined as a function of Ti-dopant (0, 7, 14, and 28%). The research focused on the effect of different Ti-dopant concentrations, and we tried to evaluate the thermal parameters using photohermal lens technique as a simple, non-contacting method. The results show an increase in the values of *D* by 5 times with an increment of Ti-dopant from 0% to 28%. The addition of Ti did not produce any additional phase in the material, although, the separation of the crystallographic planes reduced, indicating the presence of the Ti atoms in the crystal structure.**

**KEYWORDS:** $WS_2$ nanosheet, Ti-dopant, thermal lens, thermal diffusivity.

## I. INTRODUCTION

Two-dimensional (2D) semiconductors possess new properties in comparison to their bulk state [1]. Their 2D structures make them suitable materials for sensing and catalysis applications owing to their larger surface-area-to-volume ratio. Transition metal dichalcogenides (TMD) have been widely studied due to their unique and interesting properties like direct bandgap, water resistance, photoluminescence, thermoelectric properties, and good heat dissipation capability [2]–[4]. They consist of a transition metal layer sandwiched between chalcogen (S, Se, or Te) layers [5]. In 2D configuration, many of TMDs show a transition from an indirect bandgap of the bulk state to a direct bandgap of the 2D materials [2]. Because of this new electronic structure, they can have high photoluminescence and also have higher carrier mobility [6]. With these properties, 2D TMDs are good candidates for LED and field-effect transistors (FET) [7]. 2D TMDs can be developed through exfoliation (mechanical or chemical methods) [8] of bulk TMDs or directly from their raw material by the chemical vapor deposition method (CVD). The last method has the advantage of generating isolated and high-quality 2D samples in cost-effective way [9]–[11].

The two dimensional tungsten disulfide (2D-$WS_2$) has a strong spin-orbital coupling [12], a direct bandgap of 2 eV, high charge mobility, and high thermal stability [6]. It is a good candidate for many applications like hydrogen generation, sensing of humidity [13], sensing different gases like $NO_2$ and $H_2S$ [14], fluorescence enhancement [15], photodetector [16], LED or a variety of electronic devices [6], [12]. For such applications especially in microelectronic devices, heat management plays a vital role and thermal characterization of the constituent components is very important.

The electrical and optical properties of 2D TDMs are studied extensively [5], [17], [18],

[ Downloaded from ijop.ir on 2026-11-23 ]

but there are scarce experimental reports about their thermal parameters. The thermal conductivity ($\kappa$) value depends on the sample's geometry and for the same compound structure, different values are reported depending on the size and the thickness of the 2D films [4]. Most of the reports on κ measurement are done using Raman spectroscopy or thermoreflectance method [12]. In the first method, the shift in Raman peaks under laser illumination is recorded, and by using the data from Raman technique and introducing thermal modeling, κ of 2D TMD samples is extracted [2]. The errors of this technique arise from uncertainty in measuring the heat input as well as the temperature and effects of thermomechanical stress which could affect Raman bands [19]. In thermoreflectance technique, a modulated high-power exciting laser induces periodical temperature oscillations on the sample surface that will affect the reflection of the probe laser. Then, κ can be evaluated using the intensity and phase of the reflected probe beam [20]. One important drawback of this technique is the need for a smooth surface which limits its applications [21]. Photothermal lens technique, also has been used to evaluate D and κ of thin films [18,19].

Photothermal lens technique is a non-contact optical method and a promising way to measure thermal parameters of transparent or semi-transparent samples [22]–[24]. In the pump-probe photothermal lens configuration, an excitation laser is used to excite the sample and create a temperature gradient around the laser beam axis. As a result, the temperature gradient produces a refractive index gradient with an azimuthal symmetry (assuming that the excitation laser beam profile is Gaussian). Then the excited region in the sample acts like a lens named thermal lens (TL). When the probing laser beam passes through the sample, its phase is affected by the TL effect leads to a divergent or convergent beam depending on the nature of the material [25]–[27]. By using a detector and measuring the variation of the probe beam intensity at the detector position, the photothermal lens signal can be recorded. Using the temporal evolution of the TL signal, thermal diffusivity and thermal conductivity can be determined [28], [29]. One important feature of TL method is a direct evaluation of the thermal diffusivity D which is an important property when studying unsteady-state heat transfer.

In this study, 2D titanium doped tungsten disulfide (Ti-doped $WS_2$) was prepared by CVD method. $WS_2$ has directly deposited on fluorine doped tin oxide (FTO) transparent substrates and arranged to vertical nanosheets. Despite an indirect bandgap for its bulk state, it possesses a direct bandgap of 2 eV. Ti atomic radius is close to that of W, and Ti can substitute W in $WS_2$ structure forming covalence bonds with S atoms in the lattice. The first report of doping $WS_2$ by Ti was done by our group and it shows an enhancement in electronic and optical properties such as photocurrent density compared to pure $WS_2$ and Mo-doped $WS_2$ [6].

In this work, we investigate the thermo-optical properties of 2D Ti-doped $WS_2$ as a function of Ti-dopant concentration. Moreover, the morphology and structural parameters were obtained by field emission scanning electron microscopy (FESEM), UV-Vis spectrophotometry, X-ray diffraction (XRD), and energy dispersive scanning (EDS) as well as Raman Spectroscopy.

## II. THEORETICAL PART

In the TL model approach, developed by Shen *et al*. the TL signal S(z, t) is defined as the relative change of the light transmission T(z, t) through a small aperture when the excitation beam impinges on the sample [30]:

$$S(z.t) = \frac{T(z.t) - T(0)}{T(0)} \qquad (1)$$

T(0) is the transmittance when the excitation beam is off. According to this model, the TL signal can be expressed as a function of the photothermal and geometrical parameters of the sample as follows:

[ Downloaded from ijop.ir on 2026-11-23 ]

$$S(z.t) = \Phi_0 tan^{-1}\{[4m(z)v(z)\,t/t_c(z)]/[v^2(z) + [1 + 2m(z)]^2 + [1 + 2m(z) + v^2(z)]^2 2\,t/t_c(z)]\} \quad (2)$$

$$\Phi_0 = \frac{P_e \alpha l}{\lambda_p \kappa}\frac{ds}{dT} \quad (3)$$

$$m(z) = \frac{w^2{}_p(z)}{w^2{}_e(z)} \quad (4)$$

$$w_{p.e}(z) = w_{0p.0e}\sqrt{1 + \left(\frac{z - a_{p.e}}{z_{p.e}}\right)^2} \quad (5)$$

$$w_{0p.0e} = \sqrt{z_{p.e}\frac{\lambda_{p.e}}{\pi}} \quad (6)$$

$$v(z) = \frac{z - a_p}{z_p} + \frac{z_p}{L - z}\left[1 + \left(\frac{z - a_p}{z_p}\right)^2\right] \quad (7)$$

where, $\lambda_{p.e}$, $w_{p.e}(z)$, $w_{0p.0e}$, $a_{p.e}$ and $z_{p.e}$ are the wavelength, beam radii, beam waists, position of the beam waists, and Rayleigh parameters of probe and excitation beams, respectively. $P_e$, $\alpha$, $l$, $ds/dT$, $\kappa$, $t_c$, L are, the power of the excitation laser beam, absorption coefficient, sample's thickness, the temperature dependence of the optical path change, thermal conductivity, characteristic thermal lens time constant, and the distance between the sample (which is placed at $z = 0$) and the detector [31].

## III. EXPERIMENTAL PART

### A. *Samples preparation*

The substrates are 2 mm thickness glass coated with ~500 nm FTO (Dyesol Ltd.). FTO as a transparent (visible transmittance~80%) and conducting (conductivity~$3\times10^{-4}\Omega^{-1}cm^{-1}$) substrate was also used as an electrode for a further characteristics of the samples [32]. Vertical $WS_2$ nanosheets were produced by chemical vapor deposition (CVD) method using a mixture of argon/hydrogen atmosphere at a pressure of $10^{-2}$ Torr and flow rate of 40 sccm in a tube furnace. $TiO_2$, $WO_3$ (99.7%), and S powder (99.5%) were purchased from α-Aeser and used as precursors for Ti, W, and S. Different dopant concentrations are prepared by using different $TiO_2$ to $WO_3$ powders mixture in the CVD furnace. The used powders ratios are listed in Table 1. The position for $TiO_2$, $WO_3$, and S powders is defined by the maximum temperature of the points in the furnace. For $TiO_2$, $WO_3$ was at the center ($T_{max}$~500ºC) where also the substrates are placed and for S powder at the flow entrance of the furnace ($T_{max}$~180ºC). Increment of the furnace temperature for the sample deposition was done in 20 min from room temperature to 500ºC, after reaching the growth temperature at 500ºC stabilized for 3 min. The quartz tube at the end of the process is naturally cooled down to room temperature.

Table 1. Different powders mixture used to introduce different Ti-doping concentrations

| $TiO_2/WO_3$ powders ratio | Sample name |
|---|---|
| 0/100 | pure $WS_2$ |
| 5/95 | 7% Ti-doped $WS_2$ |
| 10/90 | 14% Ti-doped $WS_2$ |
| 20/80 | 28% Ti-doped $WS_2$ |

### B. *Photothermal Lens Experimental Setup*

The experimental setup is schematically shown in Fig. 1. A diode-pumped 532 nm solid-state laser (MGL-III-532-100, UltraLasers, Canada) is used as an excitation laser (EL).

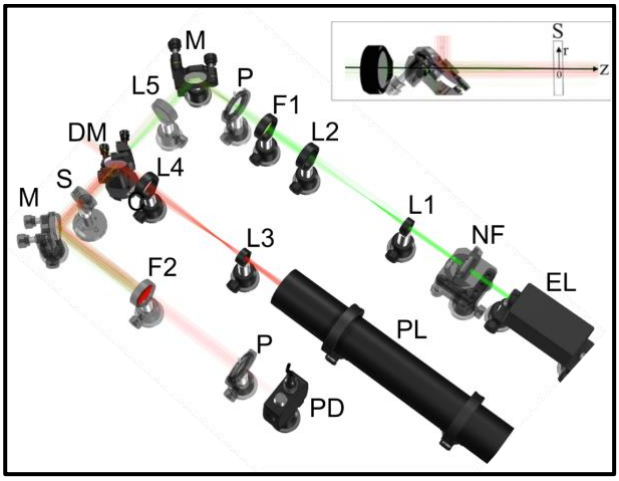


Fig. 1. Schematic of the pump-probe photothermal lens setup: EL: excitation laser, PL: probe laser, PD: photodiode, NF: neutral density filter, L1, L2, L3, L4, L5: lens, F1 and F2 band-pass filters, M: mirror, DM: dichroic mirror, P: pinhole, S: sample, the inset

[ Downloaded from ijop.ir on 2026-11-23 ]

shows the configuration regarding the z-axis and the radial direction (r) of the optical configuration.

A signal generator (RIGOL DG1022, RIGOL Technologies, Inc, USA) modulates the EL at 3 Hz. A neutral density filter (NF) (Thorlabs, NDC 50S-3) is placed after the laser to adjust the power of the EL to 24 mW on the sample. The EL is first collimated by the lenses L1 (LB1757-A, Thorlabs, USA) and L2 (LB1676-A, Thorlabs, USA) and then filtered its first harmonic 1064 nm by filter F1 (Thorlabs, NF533-17, center wavelength 532 nm). After that, the beam passes through the lens L5 (LB1437-A, Thorlabs, USA) and is focused to a 40 µm diameter spot into the sample (S). Consequently, the Rayleigh distance (3 mm) is larger than the sample length to guarantee a constant radius of the beam over the sample path length and the gradient of the heat flow to be mainly in the radial direction. The probe laser (PL), a 5 mW He-Ne laser (05-UR-111, Melles Griot, USA) is collimated by a set of lenses L3 (LB1757-A, Thorlabs, USA) and L4 (LB1676-A, Thorlabs, USA) and directed to the sample collinearly with the EL. After interacting with the sample, the PL's intensity changes are detected by the photodiode (PD) (PDA 36A-EC, Thorlabs, USA) with a 0.5 mm pinhole (P) and a 632 nm filter F2 (MELLES GRIOT, USA). The signal from the PD is measured and monitored by the oscilloscope (RIGOL DS1102E, RIGOL Technologies, Inc, USA). The inset in Fig. 1 shows the configuration regarding the excitation and probe beams propagating collinearly in the z-axis direction.

## IV. Results and Discussion

### A. *Absorbance and Structural Characterization*

The UV-Visible absorption spectra shown in Fig. 2 were measured using a Uv-Vis spectrophotometer (Pishro Pazhohesh, IR-Iran). Absorption spectra show the main absorption peaks at wavelengths: 420, 480, 540, and 650 nm. The UV-Visible absorption results indicate that higher Ti-dopant concentrations resulted in higher absorbance in the wavelength related to the excitation laser (532nm). One explanation could be that Ti-dopant tuned the structure bandgap results in absorbance enhancement.

Fig. shows the FESEM image of $WS_2$ nanosheets, which indicates their alignment vertical to the substrate. The same geometrical characteristics are seen for all samples regardless of their different doping concentrations. The surface area of the nanosheets varies from around 200 nm to 2 µm in width.

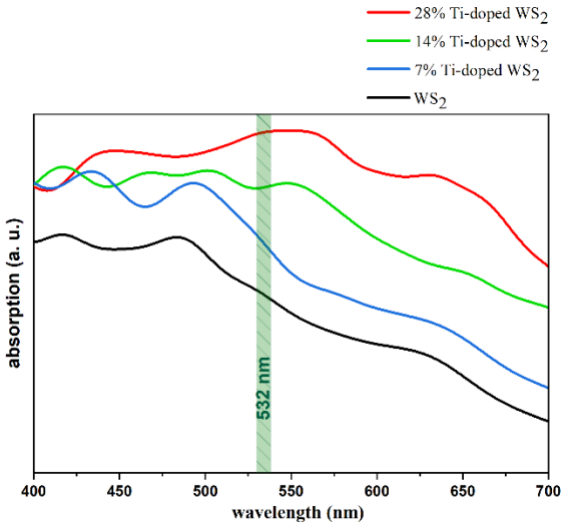


Fig. 2. UV-Visible absorption spectra for Ti-doped $WS_2$ samples at different concentrations. The green crosshatch indicate the region related to the excitation laser wavelength.

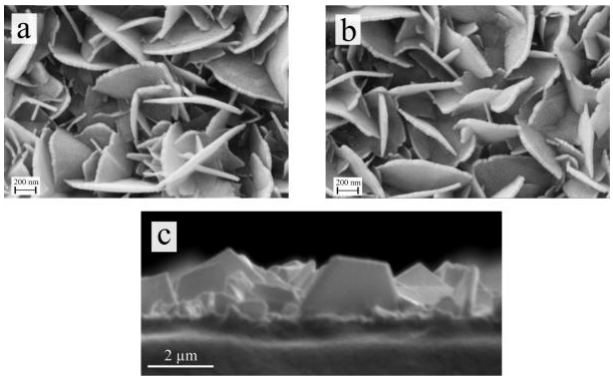


Fig. 3. FESEM image of (a) pure $WS_2$ and (b) 28% Ti-doped $WS_2$ vertical nanosheets, and (c) a side view of the 28% $WS_2$ vertical nanosheets.

Fig. shows the XRD pattern using Cu Kα radiation (Philips Netherlands). The results show that the main peak of the $WS_2$ crystal structure varies between 14 and 15 degrees (circled in Fig. 4), which corresponds to (002) crystal planes (JCPDS Card Number 98-003-

[ Downloaded from ijop.ir on 2026-11-23 ]

9096). The rest of the peaks correspond to FTO substrate. The XRD analysis ( Fig. a) of pure $WS_2$, (7%, 14% and 28% Ti-doped $WS_2$ samples) indicates no evidence of $TiO_2$ structure. Additionally, for pure $WS_2$ ( Fig. b), the peak (002) is located at 14.23º and shifts to higher degrees 14.31º, 14.39º, and 14.41º for 7%, 14%, and 28% Ti-doped $WS_2$ samples, respectively. According to Bragg's equation, this shift indicates that the d-spacing between (002) crystallographic planes decreases with increasing the Ti-dopant concentrations. The reason for this shift could be the substitution of W with Ti in the crystal structure of $WS_2$ [6].

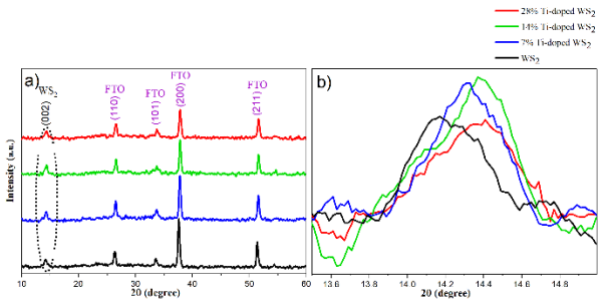


Fig. 4. XRD pattern of (a) pure, 7%, 14%, and 28% Ti-doped $WS_2$ nanosheets. The circled part corresponds to $WS_2$ peak and other peaks are related to FTO substrate, (b) characteristic XRD (002) peak of $WS_2$ crystal structure for all samples in (a).

Ionic radii for both Ti and W are close to each other but the distortion that happens to the lattice as a result of dopants causes a contraction which results in an increment of the related XRD peak [33].

To analyze the constituent elements of the samples, energy dispersive X-ray spectroscopy (EDS) has been used. Figure 5 shows the EDS for 7% and 28% Ti-doped $WS_2$ samples.

The abundances of elements in the samples are in order S, W, and then Ti as it is expected from the abundances in the composition. The defined dopant percentage in this work is calculated by the output of the EDS analysis as the ratio of Ti to W.

Raman spectroscopy analyses of the samples are shown in Fig. 6(a). The main two peaks are related to in-plane ($E^1_{2g}$) and out-of-plane ($A_{1g}$) vibrations of the sulfur atoms in the crystal structure [34]. To evaluate more accurately the information related to $A_{1g}$ peak, multiple peak fit analysis has been used (Fig. 6(b)). The $A_{1g}$ peak for the 28% Ti-doped $WS_2$ sample shifted (4 $cm^{-1}$) to higher frequencies. This result agrees with the XRD analysis which also indicates a decrease in the spacing between the (002) planes (Fig.4b). The decrease in the spacing of the out-of-plane or normal direction to the $WS_2$ sheets could be used as a confirmation for the substitution of titanium in the crystal structure [35]. The peaks between 500 and 700 $cm^{-1}$ correspond to higher order Raman modes [36].

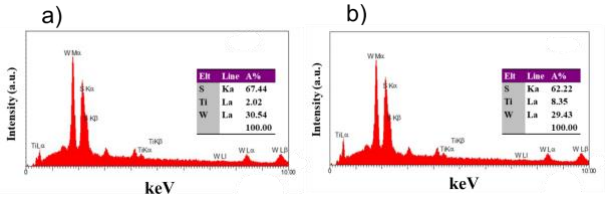


Fig. 5. EDS analysis for (a) 7% and (b) 28% Ti-doped $WS_2$ nanosheets.

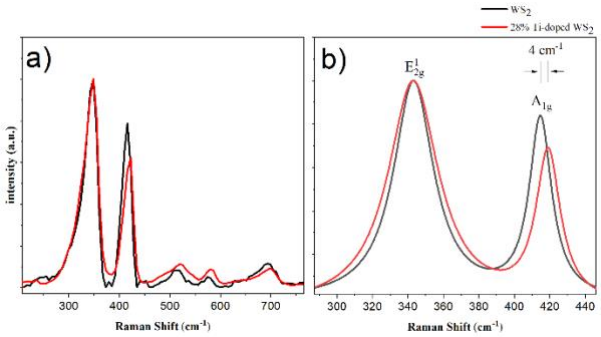


Fig. 6. (a) Raman spectra of the pure $WS_2$ and 28% Ti-doped $WS_2$ nanosheets structure. (b) the main two characteristic Raman peaks for $WS_2$ crystal structure with the 4 $cm^{-1}$ shift by using peak fit in origin software.

## B. *Photothermal lens results*

For calibrating the setup, $D$ of ethanol was measured, and the value ($0.94\times 10^{-1}\, mm^2/s$) agrees well with the literature data [37]. Subsequently, we proceed to measure Ti-doped $WS_2$ samples. The results show that increasing Ti-doping produces a higher TL signal (Fig. 7), in agreement with the UV-Vis measurement (Fig. 2).

Parameter $D$ of the samples is evaluated by the best fit to the TL experimental signals using Eq.2 for known experimental parameters such as the distance between the detector and the

[ Downloaded from ijop.ir on 2026-11-23 ]

sample, L=28.5 cm and the Rayleigh distances, $z_e$ =0.3 cm, $z_p$ = 10000 cm. Considering that the Rayleigh distance of the excitation beam is much larger than the thickness of the examined sample, the heat transfer through the sample will be mainly in the perpendicular direction to the laser beam axis and therefore, parallel to the substrate (in-plane). Note that, the value of the absorbance for the glass substrate is relatively very low in comparison to the layer of $WS_2$, therefore, the measured $D$ is mainly because of the in-plane transmission of heat. Calculated $D$ and estimated $\kappa$ using the mentioned approach are given in Table 2. For calculating $\kappa$, we have used a very-well known dependence of $D$ as reported in the reference [38].

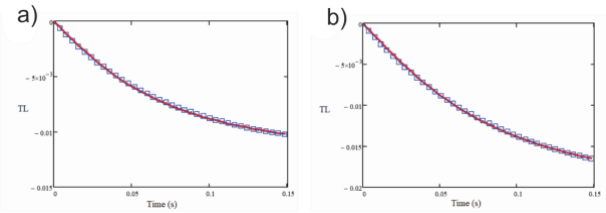


Fig. 7. TL signal as a function of time and the best-fitted curve for (a) 7% and (b) 28% Ti-doped $WS_2$ samples at 3 Hz modulation frequency. The average RSD for 3 measured values lies in the range of 8%-10%.

We could find only $\kappa$ but not $D$ of $WS_2$ nanostructures in previous studies. The values for $D$ and $\kappa$ of 2D TMDs and also bulk W reported in the literature are listed in Table 3. The reported values for $\kappa$ of 2D $WS_2$ are in the range of 1 to 50 W/m.K depend on the fabrication method and the size of the samples [12],[39]. In this study, the TL signal as well as $D$ increased with Ti-dopant concentration in $WS_2$ nanosheets. In reference [6], the evaluation of optical bandgap and photocurrent density for both the pure $WS_2$ sample and 28% Ti-doped $WS_2$ gives respectively, 1.93 and 1.69 eV for the bandgap and 32 and 175 μA/cm$^2$ for the photocurrent density under illumination power of 100 mW/cm$^2$. Therefore, in Table 2 the increment in thermal diffusivity could be related to the lower bandgap and higher carrier mobility of the Ti-doped $WS_2$ samples that have a role in the sample thermal behavior as well.

Table **2** Thermal parameters for WS2 and Ti-doped $WS_2$

| Sample name | $D$($10^{-6}$ m$^2$/s) | $\kappa$(W/m.K) |
|---|---|---|
| pure $WS_2$ | 0.24±0.03 | 0.7> |
| 7% Ti-doped $WS_2$ | 0.5±0.04 | 1 |
| 14% Ti-doped $WS_2$ | 0.8±0.07 | 2 |
| 28% Ti-doped $WS_2$ | 1.3±0.1 | 4 |

Table **3** Reported thermal conductivity and thermal diffusivity in some literature

| Sample | method | $\kappa$ (W/m.K) | $D$ (mm$^2$/s) | Ref. |
|---|---|---|---|---|
| exfoliated single layer $MoS_2$ | Raman spectroscopy | 35 | - | [38] |
| exfoliated few layers $MoS_2$ | suspended micro-devices | 44-52 | - | [38] |
| exfoliated few layers $MoS_2$ | Raman spectroscopy | 52 | - | [38] |
| single layer MoS2 | Raman spectroscopy | 84±17 | - | [40] |
| single layer $MoSe_2$ | Raman spectroscopy | 59±18 | - | [40] |
| Bulk $MoS_2$ | Time-resolved magneto-optic Kerr effect | 85-112 | - | [38] |
| single layer $WS_2$ | Raman spectroscopy | 32 | - | [12] |
| single layer $WS_2$ | Raman spectroscopy | 15, 28 | - | [41,42] |
| Double layer $WS_2$ | Raman spectroscopy | 53 | - | [12] |
| single layer $MoS_2$ | Raman spectroscopy | 34.5 | - | [43] |
| Bulk W | | 135 | 27 | [44] |

## V. CONCLUSION

Ti-doped $WS_2$ perpendicular nanosheets have been fabricated on fluorine doped tin oxide (FTO) substrates using a quasi-low temperature chemical vapor deposition (CVD) technique. Thermal lens (TL) signal measurement was

[ Downloaded from ijop.ir on 2026-11-23 ]

used to evaluate Thermal diffusivity (D) (0.24-1.3 $mm^2/s$) and thermal conductivity, $\kappa$ ($\leq$ 4 W/m.K) of Ti-doped $WS_2$ nanosheets. Higher dopant concentrations possess higher absorption, TL signal, and *D* Ti-dopants influence $WS_2$ crystal features accompanied by reduction of two dimensional (2D) layers spacing that evidence by a shift in the XRD and also Raman peaks. The results demonstrate the ability of the mode-mismatched photothermal lens technique to calculate *D* in delicate thin films. These measurements are important for photonic devices, to design the proper heat removal system which is critical to avoiding thermal lensing and other deleterious effects on the device application induced by the temperature gradient.

## ACKNOWLEDGMENTS

The authors would like to express gratitude to ICTP for support of this work through the Associateship Scheme and TRIL Programs, and in particular, the SPIE-ICTP Anchor Research Program funded generously by the International Society for Optics and Photonics (SPIE). Also, the authors thank the Shahid Chamran University of Ahvaz for supporting this research with grant number SCU.SP99.559.

## REFERENCES

**[1]** W. Cai, A.L. Moore, Y. Zhu, X. Li, S. Chen, L. Shi, and R.S. Ruoff, "Thermal transport in suspended and supported monolayer graphene grown by chemical vapor deposition," Nano Lett. Vol. 10, pp. 1645-1651, 2010.

**[2]** L. Liu, H. Yao, H. Li, Z. Wang, and Y. Shi, "Recent advances of low-dimensional materials in lasing applications," FlatChem, Vol. 10, pp. 22-38, 2018.

**[3]** M. Nurunnabi and J. McCarthy, *Biomedical applications of graphene and 2D nanomaterials*, Elsevier, Cambridge, CA, 2019.

**[4]** Z. Zhang, Y. Xie, Y. Ouyang, and Y. Chen, "A systematic investigation of thermal conductivities of transition metal dichalcogenides," Int. J. Heat Mass Transf. Vol. 108, pp. 417-422, 2017.

**[5]** J. N. Coleman, M. Lotya, A. O'Neill, S. D. Bergin, P.J. King, U. Khan, K. Young, A. Gaucher, S. De, R. J. Smith,"Two-dimensional nanosheets produced by liquid exfoliation of layered materials," Science, Vol. 331, pp. 568-571, 2011.

**[6]** A. Ahmadi and M.Z. Shoushtari, "Enhancing the photoelectrochemical water splitting performance of $WS_2$ nanosheets by doping titanium and molybdenum via a low temperature CVD method," J. Electroanal. Chem. Vol. 849, pp. 113361 (1-8), 2019.

**[7]** W. Yin, X. Bai, P. Chen, X. Zhang, L. Su, C. Ji, H. Gao, H. Song, and W.W. Yu, "Rational control of size and photoluminescence of $WS_2$ quantum dots for white light-emitting diodes," ACS Appl. Mater. Interfaces, Vol. 10, pp. 43824-43830, 2018.

**[8]** O.Y. Posudievsky, O.A. Khazieieva, A.S. Kondratyuk, V.V. Cherepanov, G.I. Dovbeshko, V.G. Koshechko, and V.D. Pokhodenko, "Liquid exfoliation of mechanochemically nanostructured tungsten disulfide to a graphene-like state," Nanotechnology, Vol. 29, pp. 085704 (1-7), 2018.

**[9]** Z. Cai, B. Liu, X. Zou, H. and M. Cheng, "Chemical vapor deposition growth and applications of two-dimensional materials and their heterostructures," Chem. Rev. Vol. 118, pp. 6091-6133, 2018.

**[10]** H. Yan, J. Li, D. Liu, X. Jing, D. Wang, and L. Meng, "Controlled preparation of high quality WS 2 nanostructures by a microwave-assisted solvothermal method," Cryst. Eng. Comm. Vol. 20, pp. 2324-2330, 2018.

**[11]** C. Cong, J. Shang, X. Wu, B. Cao, N. Peimyoo, C. Qiu, L. Sun, and T. Yu, "Synthesis and optical properties of large-area single-crystalline 2D semiconductor $WS_2$ monolayer from chemical vapor deposition," Adv. Opt. Mater. Vol. 2, pp. 131-136, 2014.

**[12]** N. Peimyoo, J. Shang, W. Yang, Y. Wang, C. Cong, and T. Yu, "Thermal conductivity determination of suspended mono-and bilayer WS 2 by Raman spectroscopy," Nano Res. Vol. 8, pp. 1210-1221, 2015.

**[13]** M.A. Dwiputra, F. Fadhila, C. Imawan, and V. Fauzia, "The enhanced performance of capacitive-type humidity sensors based on ZnO nanorods/$WS_2$ nanosheets heterostructure," Sens. Actuators B Chem. Vol. 310, pp. 127810 (1-13), 2020.

[ Downloaded from ijop.ir on 2026-11-23 ]

**[14]** D. Liu, Z. Tang, and Z. Zhang, "Comparative study on $NO_2$ and $H_2S$ sensing mechanisms of gas sensors based on $WS_2$ nanosheets," Sens. Actuators B Chem. Vol. 303, pp. 127114 (1-7), 2020.

**[15]** B. Rai, P.V. Sarma, V. Srinivasan, M.M. Shaijumon, and S.S. Ramamurthy, "Engineering of Exciton–Plasmon Coupling Using 2D-$WS_2$ Nanosheets for 1000-Fold Fluorescence Enhancement in Surface Plasmon-Coupled Emission Platforms," Langmuir, Vol. 37, pp. 1954-1960, 2021.

**[16]** J. Li, J. Han, H. Li, X. Fan, and K. Huang, "Large-area, flexible broadband photodetector based on $WS_2$ nanosheets films" Mater Sci Semicond Process,Vol. 107, pp. 104804 (1-6), 2020.

**[17]** S.J. Varma, J. Kumar, Y. Liu, K. Layne, J. Wu, C. Liang, Y. Nakanishi, A. Aliyan, W. Yang, and P.M. Ajayan, "2D $TiS_2$ layers: a superior nonlinear optical limiting material," Adv. Opt. Mater. Vol. 5, pp. 1700713 (1-9), 2017.

**[18]** J. Jadczak, L. Bryja, J. Kutrowska-Girzycka, P. Kapuściński, M. Bieniek, Y. Huang, and P. Hawrylak, "Room-temperature multi-phonon upconversion photoluminescence in monolayer semiconductor $WS_2$," SPIE OPTO, 2020, California, USA, Vol. 112980K, pp. 1-10, 2020.

**[19]** T. Beechem, L. Yates, and S. Graham, "Invited Review Article: Error and uncertainty in Raman thermal conductivity measurements," Rev. Sci. Instrum. Vol. 86, pp. 041101 (1-11), 2015.

**[20]** A.A. Graf, *Physical and chemical characterisation of exfoliated layered nanomaterials*, PhD Diss. University of Sussex, 2020.

**[21]** S. Sandell, E. Chavez-Angel, A. El Sachat, J. He, C.M. Sotomayor Torres, and J. Maire, "Thermoreflectance techniques and Raman thermometry for thermal property characterization of nanostructures," J. Appl. Phys. Vol. 128, pp. 131101 (1-25), 2020.

**[22]** H. Cabrera, I. Ashraf, F. Matroodi, E.E. Ramírez-Miquet, J. Akbar, J.J. Suárez-Vargas, J.B. Ramírez, D. Korte, H. Budasheva, and J. Niemela, "Photothermal lens technique: a comparison between conventional and self-mixing schemes," Laser Phys. Vol. 29, pp. 055703 (1-5), 2019.

**[23]** S.E. Bialkowski, N.G. Astrath, and M.A. Proskurnin, *Photothermal Spectroscopy Methods*, John Wiley & Sons, 2019.

**[24]** H. Cabrera, D. Mendoza, J. Benítez, C.B. Flores, S. Alvarado, and E. Marín, "Thermal diffusivity of few-layers graphene measured by an all-optical method," J. Phys. D, Vol. 48, pp. 465501 (1-5), 2015.

**[25]** M. Proskurnin, D. Volkov, T. Gor'kova, S. Bendrysheva, A. Smirnova, and D. Nedosekin, "Advances in thermal lens spectrometry," J. Anal. Chem. Vol. 70, pp. 249-276, 2015.

**[26]** A. Smirnova, M.A. Proskurnin, K. Mawatari, and T. Kitamori, "Desktop near-field thermal-lens microscope for thermo-optical detection in microfluidics," Electrophoresis, Vol. 33, pp. 2748-2751, 2012.

**[27]** H. Ono, K. Takeda, and K. Fujiwara, "Thermal lens produced in a nematic liquid crystal," Appl. Spectrosc. Vol. 49, pp. 1189-1192, 1995.

**[28]** M. Liu and M. Franko, "Thermal lens spectrometry: still a technique on the horizon?," Int. J. Thermophys. Vol. 37, pp. 1-16, 2016.

**[29]** M. Galkin, Y.V. Ageeva, D. Nedosekin, M. Proskurnin, A.Y. Olenin, and G. Mokrousov, "Thermal lens spectrometry for the synthesis and study of nanocomposites on the basis of silver salts absorbed by a polyacrylate matrix," Mosc. Univ. Chem. Bull. Vol. 65, pp. 91-97, 2010.

**[30]** J. Shen, R.D. Lowe, and R.D. Snook, "A model for cw laser induced mode-mismatched dual-beam thermal lens spectrometry," Chem. Phys. Vol. 165, pp. 385-396, 1992.

**[31]** A. Marcano, H. Cabrera, M. Guerra, R.A. Cruz, C. Jacinto, and T. Catunda, "Optimizing and calibrating a mode-mismatched thermal lens experiment for low absorption measurement," J. Opt. Soc. Amer. B, Vol. 23, pp. 1408-1413, 2006.

**[32]** M. Chowdhury, K.S. Rahman, V. Selvanathan, A.M. Hasan, M. Jamal, N.A. Samsudin, M. Akhtaruzzaman, N. Amin, and K. Techato, "Recovery of FTO coated glass substrate via environment-friendly facile recycling perovskite solar cells," RSC Adv. Vol. 11, pp. 14534-14541, 2021.

**[33]** Source: Web Elements [http://www.webelements.com/]

[ Downloaded from ijop.ir on 2026-11-23 ]

**[34]** S. Qiao, H. Yang, Z. Bai, G. Peng, and X. Zhang, *Identifying the number of $WS_2$ layers via Raman and photoluminescence spectrum*, Atlantis Press. Pp. 1408-1413, 2017.

**[35]** A. Ahmadi, M.Z. Shoushtari, and M. Farbod, "Photoelectrochemical application of WS 2 nanosheets prepared via a low-temperature CVD method," J. Mater. Sci.: Mater. Electron. Vol. 30, pp. 6342-6349, 2019.

**[36]** F. Wang, *Raman and Photoluminescence Spectroscopic Studies of the Micromechanics of $WS_2$ Nanocomposites*, The University of Manchester (United Kingdom), PhD Diss. 2018.

**[37]** M. Benitez, A. Marcano, and N. Melikechi, "Thermal diffusivity measurement using the mode-mismatched photothermal lens method," Opt. Eng. Vol. 48, pp. 043604 (1-8), 2009.

**[38]** J. Liu, G-M. Choi, and D.G. Cahill, "Measurement of the anisotropic thermal conductivity of molybdenum disulfide by the time-resolved magneto-optic Kerr effect" J. Appl. Phys. Vol. 116, pp. 233107 (1-6), 2014.

**[39]** J.-Y. Kim, S.-M. Choi, W.-S. Seo, and W.-S. Cho, "Thermal and electronic properties of exfoliated metal chalcogenides," Bulletin Kor. Chem. Soc. Vol. 31, pp. 3225-3227, 2010.

**[40]** X. Zhang, D. Sun, Y. Li, G-H. Lee, X. Cui, D. Chenet, Y. You, T.F. Heinz, and J.C. Hone, "Measurement of lateral and interfacial thermal conductivity of single-and bilayer $MoS_2$ and $MoSe_2$ using refined optothermal Raman technique," ACS Appl. Mater. Interfaces. Vol. 7, pp. 25923-25929, 2015.

**[41]** Y. Zhang, Q. Lv, A. Fan, L. Yu, H. Wang, W. Ma, X. Zhang, and R. Lv, "Substrate effect on thermal conductivity of monolayer $WS_2$: Experimental measurement and theoretical analysis,". arXiv preprint arXiv, Vol. 2108, pp. 13252 (1-33), 2021.

**[42]** Y. Zhang, Q. Lv, A. Fan, L. Yu, H. Wang, W. Ma, R. Lv, and X. Zhang, "Reduction in thermal conductivity of monolayer $WS_2$ caused by substrate effect," Nano Res. pp. 1-10, 2022.

**[43]** R. Yan, J.R. Simpson, S. Bertolazzi, J. Brivio, M. Watson, X. Wu, A. Kis, T. Luo, A.R. Hight Walker, and H.G. Xing, "Thermal conductivity of monolayer molybdenum disulfide obtained from temperature-dependent Raman spectroscopy," ACS Nano, Vol. 8, pp. 986-993, 2014.

**[44]** J. Habainy, Y. Dai, Y. Lee, and S. Iyengar, "Thermal diffusivity of tungsten irradiated with protons up to 5.8 dpa," J. Nucl. Mater. Vol. 509, pp. 152-157, 2018.



**Fatima Matroodi** received her Ph.D. in 2015 from Shahid Beheshti University. In 2016 she joined Shahid Chamran University as an academic member. Her research interests are different laser spectroscopic techniques including Raman spectroscopy, photothermal lens spectrometry, Laser Induced Breakdown Spectroscopy (LIBS) and fluorescence spectroscopy.



**Ali Ahmadi** was born in Borujen, Iran, on September 18, 1978. He received the B.S. in physics in 2001 from Isfahan University, Isfahan, Iran, and the M.S. degree in solid state physics in 2006 from Shahid Chamran University of Ahvaz, Ahvaz, Iran. He obtained the Ph.D. degree in Experimental Solid State Physics in 2019 from Shahid Chamran University of Ahvaz, Ahvaz, Iran. He is a Research Fellow in the field of Photoelectrochemical water splitting.

[ Downloaded from ijop.ir on 2026-11-23 ]



**Morteza Zargar Shoushtari** received his Ph.D. degree in 1983 from Southern Illinois University Carbondale of USA. He is a professor of Physics at Shahid Chamran University of Ahvaz. His research interests are condensed matter physics, nanomaterials, cystography, solar cells, low temperature physics, magnetic materials. He has published four books, 104 journal papers, and 167 conference papers.



**Humberto Cabrera** graduated in physics from the ST Kliment Ojhridski University of Sofia, Bulgaria, obtained the master degree in Optics from the ISPJAE University, Havana and the Ph.D degree in Optics from the Venezuelan Institute for Scientific Research. He is currently Researcher at the Abdus Salam International Centre for Theoretical Physics (ICTP) and Istituto Nazionale di Fisica Nucleare (INFN). Currently, his research activities are directed to the development of photothermal and laser-based methods for thermo-optical characterization of materials, identification and determination of toxic compounds in the environment as well as the investigation of photocatalytic degradation of pollutants in water. Additionally, his research topics covered the implementation of on-line thermal lens detection for electrophoresis techniques applied in separation and detection of nanoparticles and biomolecules using electrophoresis coupled with thermal lens spectrometry. Dr Cabrera has been active in development of solid state laser system used for spectroscopy of muonic hydrogen. He holds 90 publications with more than 800 citations and two patents related to the fields of photothermal science and self-mixing interferometry.

[ Downloaded from ijop.ir on 2026-11-23 ]